Enhancement of the spin Hall voltage in a reverse-biased planar *p-n* junction

L. Nádvorník,[1,2,*] K. Olejník,[1] P. Němec,[2] V. Novák,[1] T. Janda,[2,1] J. Wunderlich,[1,3] F. Trojánek,[2] and T. Jungwirth[1,4]

[1]*Institute of Physics ASCR, v.v.i., Cukrovarnická 10, 16253 Praha 6, Czech Republic*

[2]*Faculty of Mathematics and Physics, Charles University, Ke Karlovu 3, 12116 Praha 2, Czech Republic*

[3]*Hitachi Cambridge Laboratory, J. J. Thomson Avenue, CB3 0HE Cambridge, United Kingdom*

[4]*School of Physics and Astronomy, University of Nottingham, Nottingham NG7 2RD, United Kingdom*

(Received 13 May 2016; revised manuscript received 12 July 2016; published 11 August 2016)

We report an experimental demonstration of a local amplification of the spin Hall voltage using an expanding depletion zone at a *p-n* junction in GaAs/AlGaAs Hall-bar microdevices. It is demonstrated that the depletion zone can be spatially expanded by applying reverse bias by at least 10 μm at low temperature. In the depleted regime, the spin Hall signals reached more than one order of magnitude higher values than in the normal regime at the same electrical current flowing through the microdevice. It is shown that the *p-n* bias has two distinct effects on the detected spin Hall signal. It controls the local drift field at the Hall cross which is highly nonlinear in the *p-n* bias due to the shift of the depletion front. Simultaneously, it produces a change in the spin-transport parameters due to the nonlinear change in the carrier density at the Hall cross with the *p-n* bias.

DOI: 10.1103/PhysRevB.94.075306

I. INTRODUCTION

During the last decade, the direct and inverse spin Hall effects (SHE) [1–6] have been established as important tools in a wide variety of spintronic structures, where they act as generators or detectors of spin polarized currents in semiconductors and metals [1–7], in systems with a ferromagnetic layer as a trigger of magnetization reversal [8,9], or as electric polarimeters sensitive to the helicity of incoming light [10,11]. Recently, significant attention has been also focused on concepts of logical spintronic devices based on the inverse spin Hall effect (ISHE) [7]. In these proposals, the output ISHE signals are altered either using variations in the longitudinal drift biases [11,12], or by using electric gates [13].

In this paper, we make use of both approaches by employing a depleted zone created by a lateral *p-n* junction in a two-dimensional electron gas (2DEG). We benefit from the fact that in the low-dimensional structures, unlike the bulk systems, the electrostatic depletion can be highly expanded in space by several microns by applying bias across a *p-n* junction [14]. In such a two-terminal transistor [15], the relationship between the *p-n* bias and the local drift field at a Hall cross can be highly nonlinear due to the propagation of the depletion front. The presented results show that this unique transistorlike effect amplifies the ISHE voltages, detected at a series of Hall crosses, by more than a factor of 30 with respect to a normal drift bias without the depletion effect.

It is shown that the position of the depletion front can be controlled with a submicrometer resolution by the *p-n* bias. Consistently with the previously reported observation [16], we will finally discuss the spin-related parameters with respect to the carrier depletion due to the voltage applied across the *p-n* junction.

II. SETUP AND SAMPLE

The experiments were performed on an AlGaAs/GaAs-based heterostructure containing a 2DEG and a quasilateral *p-n* junction, as sketched in Fig. 1(a). A sequence of a silicon-doped $Al_{0.3}Ga_{0.7}As$ layer (580 nm, Si δ-doping density $n_{Si} = 9 \times 10^{11}$ cm^{-2}) and an undoped GaAs layer (90 nm) was deposited by molecular beam epitaxy on top of a semi-insulating GaAs substrate. The 2DEG, formed between these layers, had the moderate low-temperature mobility $\mu \approx 1.6 \times 10^4$ cm^{2}V^{-1}s^{-1} and the sheet electron density $n \approx 8 \times 10^{11}$ cm^{-2} after the light illumination. On top of it another carbon-doped GaAs layer (50 nm, C bulk doping density $n_C = 2 \times 10^{18}$ cm^{-3}) was deposited to create the *p* region, followed by an undoped GaAs capping layer (10 nm). The last two layers were wet-etched out [17] from a part of a sample surface in order to create an *n* region containing the unperturbed 2DEG with a quasilateral *p-n* junction at the etching edge [the red dashed curve in Fig. 1(a) and the contrast line in the scanning electron microscope image in Fig. 1(b)]. Both the *p* and *n* regions were contacted using the Au/Cr and AuGeNi metalization via the lift-off technique, respectively, which allowed us to apply a bias voltage over the *p-n* junction. The corresponding I/V characteristic of the *p-n* junction is plotted in Fig. 2(d), where the forward (positive) and reverse (negative) diodelike biasing regimes are clearly distinguishable. Here, V_{bias} and I_{dc} are the voltage bias between the *p* and *n* regions and the dc current flowing through the system, respectively. We performed experiments at 10 K where the quasilateral *p-n* junction shows excellent rectifying characteristics.

In order to accomplish the anticipated ISHE measurements, the heterostructure was surface patterned as depicted in Figs. 1(b) and 1(c). The Hall-bar design of marked dimensions was dry etched in such a way that its left opening was positioned over the *p-n* junction [the red dashed line in Fig. 1(c)]. The three Hall crosses (HCs) along the Hall bar, HC 1, HC 2, and HC 3, were located at distances of 2, 5, and 8 μm away from the edge of the *p-n* junction and allowed us to observe the expansion of the depleted zone through the bar when the system is reverse biased. Effects discussed in the following sections have been consistently observed in several microdevices fabricated from the same wafer and from different wafers of similar nominal composition.

The measurement setup is shown in Fig. 1(d). It combines the optical spin injection via the optical orientation and the

*nadvl@fzu.cz

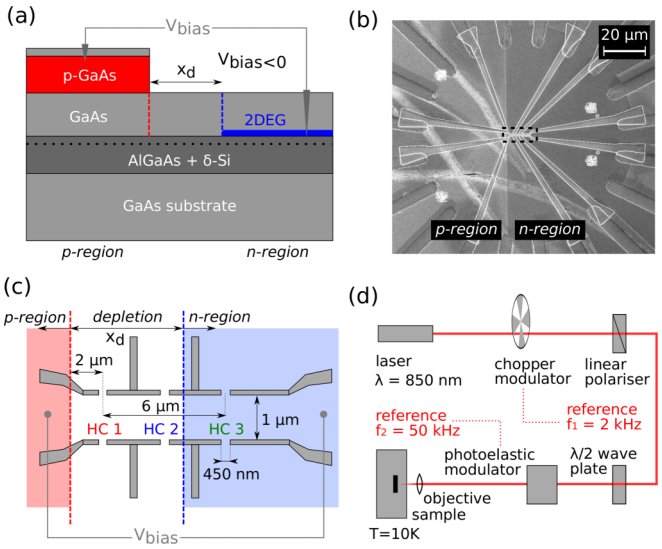

FIG. 1. (a) The layer composition of the sample, showing the created 2DEG (blue layer) and the p-doped layer (red layer). The Si δ-doping layer and the formed p-n junction at $V_{\text{bias}} = 0$ are depicted by the black dotted and red dashed lines, respectively, and x_d is the width of the depleted zone for a significant reverse bias $V_{\text{bias}} < 0$, denoted by the blue dashed line. (b) A microimage from a scanning electron microscope of the device showing the p and n regions as the areas with different shades of gray. (c) The sketch of the device design with depicted Hall crosses and dimensions [the region highlighted by the black dashed line in (b)]. The red and blue dashed lines represent the edges of the depletion region and the red and blue areas the p and n regions, respectively, corresponding to (a). The sketch is not to scale. (d) The experimental setup with its two modulators: the chopper modulator and the PEM, operating at reference frequencies f_1 and f_2, respectively.

lock-in electrical detection of the ISHE voltage [10,11,18]. A continuous-wave Ti:sapphire laser is used to generate laser light of wavelength 850 nm, the polarization of which is, after setting its intensity to 100 μW, changed to circular by a set of a linear polarizer, a $\lambda/2$ wave plate, and a photoelastic modulator (PEM) operated in the $\lambda/4$ mode. The light is then collected by a high-quality infrared objective with 20× magnification and focused by it to the sample surface, where it forms a Gaussian spot with full width at half maximum (FWHM) $w \sim 2$ μm (estimated by the scanning knife-edge technique [19]). The objective is placed on a three-dimensional (3D) piezoelectric stage that facilitates scanning the laser spot over the device with a submicrometer precision. The real time spot position with respect to the device was monitored by a CCD camera on a laser beam back-reflected from the sample. The light was double modulated by the intensity modulator (the chopper wheel) and PEM (switching of the circular polarization between the clockwise σ_+ and counterclockwise helicity σ_-), operating at frequencies $f_1 = 2$ and $f_2 = 50$ kHz, respectively. The double modulation technique enabled us to measure simultaneously the photocurrent I_{pc} at frequency f_1, which refers to the light-induced variations of the dc current I_{dc} due to the generation of extra photocarriers, and the ISHE voltages at f_2, which are dependent on the helicity of the circular polarization of the incoming light.

III. RESULTS

It has been shown theoretically and experimentally [14,20] that the depletion of planar reverse-bised p-n junctions can exceed 10 μm, unlike p-n interfaces in bulk systems where the widths of depleted zones are rather in submicrometer scales. In our device, the range of the expanding depleted region with increasing reverse bias V_{bias} is detected by sensing the dc longitudinal voltage V_{xx} between HCs along the Hall bar (Fig. 2(a) and sketch herein). We observe that for $V_{\text{bias}} > -8$ V the potential drop is located on the p-n junction which does not yet expand towards the HC 1. When V_{bias} is set below -8 V, however, V_{xx} increases significantly to potential differences of the order of hundreds of mV due to the expansion of the depleted zone through the bar. These values represent a more than 10× higher potential drop along the Hall bar than in the case of $V_{\text{bias}} > 0$, if we set the maximal current to $I_{dc} \approx 10$ μA flowing through the device [compare with Fig. 2(d)].

The advancing propagation of the depletion zone over the Hall bar is depicted by V_{xx}, measured between different HCs. The potential drop between the HC 1 and HC 3, $V_{\text{HC1}-\text{HC3}}$, shows two changes of its slope for the reverse bias: first, the signal increases rapidly when the edge of the depleted zone expands over the HC 1, and second, when the edge passes over the HC 3 and exits the bar. While the slope after the second change is associated directly with the depleted regime, the slope between the first and the second one is, in addition, affected by the propagation of the depletion edge and represents the transition regime (this observation is also discussed in the following section). Consistently, the potential difference $V_{\text{HC1}-\text{HC2}}$ shares the same evolution when the edge passes over the HC 1, but the second change in slope occurs exactly at the HC 2. Analogously, $V_{\text{HC2}-\text{HC3}}$ increases when the edge expands into the HC 2 and indicates its exit through the HC 3. The observation allowed us to indicate the position of the depletion edge with respect to a given HC as a function of V_{bias} (vertical dashed lines in Fig. 2).

In order to measure the ISHE voltage V_{xy}, collected at the three HCs at reference frequency f_2 [see Fig. 2(b) and the inset in Fig. 2(a)], the circularly polarized light spot is positioned over the corresponding HC which generates locally a spin-polarized current via the optical orientation [18]. The ISHE signals V_{xy} are enhanced abruptly when the edge of the depleted zone expands to the corresponding HC, as the spin-polarized photocurrent is dramatically increased by the presence of the high potential drop [Fig. 2(c)]. The positions of these steep changes in V_{xy} correspond well with the depletion characteristics seen in Fig. 2(a). These successive switchings on the ISHE crosses correspond to a signal amplification by a factor of ~30 at a fixed amplitude of $I_{dc} = 10$ μA [compare the inset in Fig. 2(b)].

When the depletion edge passes over a HC, the corresponding V_{xy} tends to saturate even though V_{xx} and, thus, the photocurrent increase further [21]. This behavior in similarly high electric fields has been already reported in Ref. [22]. Here, the saturation is explained by the reduction of the spin-life time τ_s due to the enhancement of the Dyakonov-Perel relaxation mechanism for higher k vectors of photocarriers [1,23], which plays even a more important role in our higher mobility system.

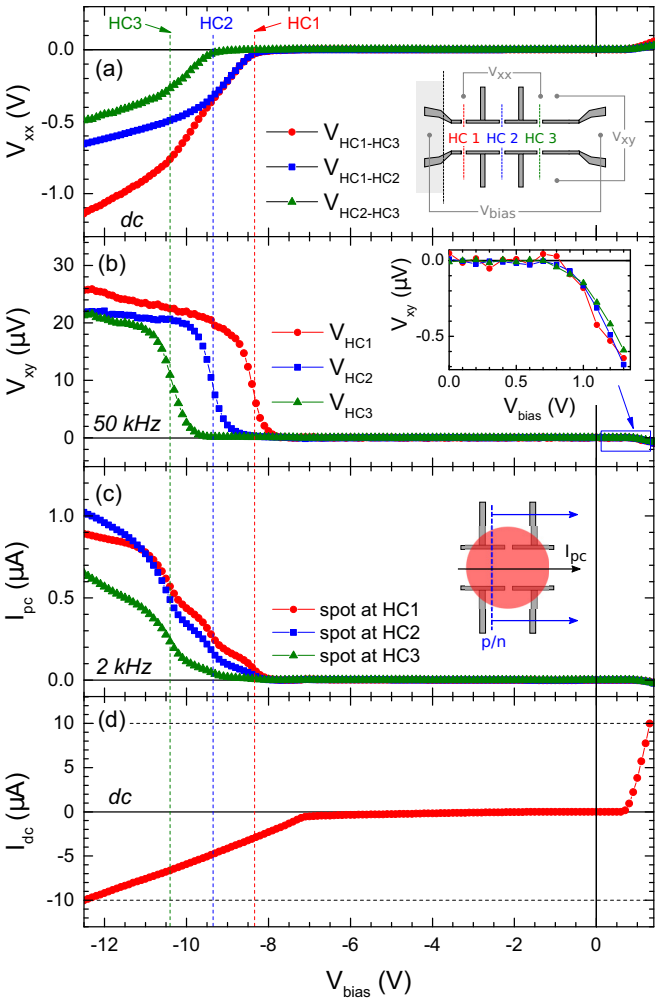

FIG. 2. (a) The dc longitudinal potential drop V_{xx}, measured between the HCs indicated in the panel, with respect to the overall bias V_{bias}. The bias values corresponding to the situation when the p-n front is propagating through each HC are depicted by the vertical dashed lines. The laser spot was positioned on the HC 2. Inset: The scheme of the electrical detection of V_{xx}, V_{xy}; the dc current I_{dc}, and the ac photocurrent I_{pc} (sensed at the reference frequency f_1) are detected between the same contacts that are used to apply V_{bias}. (b) The ISHE voltages V_{xy} detected at corresponding HCs at the reference frequency f_2 with respect to V_{bias}. The laser spot was positioned on the corresponding HC for each measurement. Inset: The detail of the dependence for $V_{\text{bias}} > 0$. (c) The I_{pc} as a function of V_{bias} for different laser spot positions. Inset: The sketch explaining the role of the propagation of the depletion front to the overall I_{pc}. (d) The dependence of I_{dc} on V_{bias}, i.e., an I/V characteristic of the p-n junction, with the spot located on the HC 2. The horizontal dashed lines represent the maximal current amplitude flowing through the device (10 μA).

The motion of the depleted zone edge can be also observed in the comparison of the bias conditions where V_{xy} and I_{pc} start to increase significantly [Figs. 2(b) and 2(c)]. The abrupt amplification of V_{xy} tends to occur at higher V_{bias} then the increase of I_{pc}. The effect is well apparent in measurements at the HC 3.

This relative shift with respect to V_{bias} can be explained if the spin drift length $l_s = E_{xx}\mu\tau_s$ is smaller than the size w of the light spot, where $E_{xx} = V_{\text{HC1-HC3}}/6\,\mu$m is the average electric field in the Hall bar in the depleted regime. Following the inset sketch in Fig. 2(c), the strong contribution to I_{pc} occurs when the depleted zone edge expands over the illuminated area. The spin-polarized carriers, however, lose their spins before they reach the region that the HC is sensitive to (a square of a size of 1 μm centered at the HC) and do not contribute to the ISHE signal. The V_{xy} is amplified when the depleted zone is expanded further towards the HC, causing a relative shift between V_{xy} and I_{pc}. The discussed effect is not strong in measurements at the HC 1, since the HC 1 is located close to the physical edge of the planar p-n junction. In order to get a rough estimate of τ_s, we use the values of $\mu \approx 1.6 \times 10^4\ \text{cm}^2\text{V}^{-1}\text{s}^{-1}$, $w \approx 2\ \mu$m, and $E_{xx} \approx 10^5\ \text{Vm}^{-1}$, giving $\tau_s < 13$ ps. This magnitude of τ_s supports the assumption of the efficient spin-relaxation mechanism, discussed in the previous paragraph.

More details of the measured ISHE signals are shown in Fig. 3. The ISHE nature of the signal V_{xy} has been carefully verified by a set of measurements with a varying degree of the circular polarization (DCP) [24] of the light. The excellent linearity of V_{xy} with DCP, an example of which is shown in

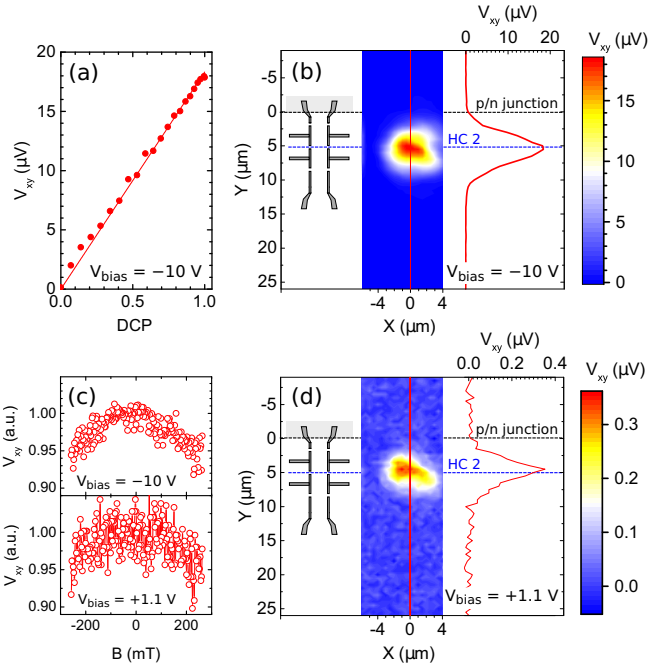

FIG. 3. (a) The dependence of V_{xy}, measured at the HC 2 and $V_{\text{bias}} = -10$ V, with respect to the degree of circular polarization (DCP). The linear trend is a check of the ISHE nature of the measured signals. (b) The 2D response of the HC 2: V_{xy} is measured at HC 2 and $V_{\text{bias}} = -10$ V with respect to the 2D position of the circularly polarized laser spot with the size $\sim$2 μm. The map shows the local character of the measured signal and no observable nonlocal (drift/diffusion) contributions. Insets: Sketches of the Hall-bar device (not to scale) and 1D sections along the red line over the 2D maps. (c) Measurements of V_{xy} with respect to the in-plane magnetic field B for $V_{\text{bias}} = -10$ and $+1.1$ V. (d) The 2D response of the HC 2 to the spot position, measured analogously to (b) for $V_{\text{bias}} = +1.1$ V.

Fig. 3(a) for HC 2 and $V_{\text{bias}} = -10$ V, is a demonstration that the measured signal is free of electrical/optical artifacts.

Considering the above inferred $l_s < w$, the spatial dependence of the ISHE signal is expected to be governed by the Gaussian profile of the laser spot. Indeed, the local character of the ISHE voltage generation can be observed on its 2D spatial dependences [see Figs. 3(b) and 3(d)]. Here, the V_{xy} was detected at the HC 2 with respect to the 2D position of the laser spot at $V_{\text{bias}} = -10$ and $+1.1$ V, i.e., $E_{xx} \approx 10^5$ and 4×10^3 Vm^{-1}, respectively. The highly localized, symmetrical and comparable ISHE responses for both bias conditions again illustrate that the spin current is localized within the laser spot size even at high electric drift fields, confirming that τ_s is of the order of 10s of picoseconds. The contribution of a longitudinal diffusive spin transport is not identified, as it would contribute to the one-dimensional (1D) profile of the ISHE signal with an odd symmetry with respect to the center of the HC, as shown in Ref. [11].

The estimated magnitude of τ_s is also consistent with the results of the measurements in the in-plane magnetic field at $V_{\text{bias}} = -10$ and $+1.1$ V [see Fig. 3(c)] [25]. Since the ISHE signal is not significantly reduced in the whole range of the accessible in-plane magnetic fields B of up to 250 mT, we infer that the spin-orbit fields dominate over the external field, giving the upper bound of the estimate of $\tau_s \ll 100$ ps (we note that $\tau_s = 100$ ps would correspond to the decrease of the signal to $1/2$ at $B = 250$ mT in the absence of the spin-orbit field; however, we observe only a decrease by $\sim$5%) [18].

IV. DISCUSSION

The Joule heating is one of the limiting factors in highly integrated electrical structures. It scales with the dc current as $\sim I_{dc}^2/\sigma$, where $\sigma = en\mu$ is the electrical sheet conductivity and e the elementary electric charge. Hence, the efficient suppression of the Joule heating in a uniform channel requires high σ. However, the detected ISHE voltage is [26–28]

$$V_{xy} = \frac{\alpha_{\text{SH}} I_s}{\sigma}, \tag{1}$$

where $\alpha_{\text{SH}} = I_{xy}/I_s$ is the spin Hall angle, I_{xy} the transverse charge current due to the ISHE, and I_s is the spin-polarized charge current generated by the drift electric field. It means that the high ISHE signal requires low σ due to the denominator in Eq. (1) and due to the fact that the low σ allows for higher I_s (low σ means a higher potential drop which accelerates more the injected photocarriers). These competing requirements on σ can be solved by having a local depletion in the Hall cross area so that the low σ is localized at the ISHE detection point while the rest of the transport channel has still high σ keeping the total Joule heating low. We show experimentally this approach using our device in the results in Fig. 2(b). Comparing the sensed V_{xy} at a fixed current amplitude $I_{dc} = 10$ μA, the ISHE signal is amplified by more than a factor of 30 in the depleted ($V_{\text{bias}} = -12$ V) regime with respect to the normal regime without the effect of the depletion ($V_{\text{bias}} = +1.3$ V). The latter regime represents the standard detection of V_{xy} in the drift regime, the values of which usually reach microvolts or less [11,13,22].

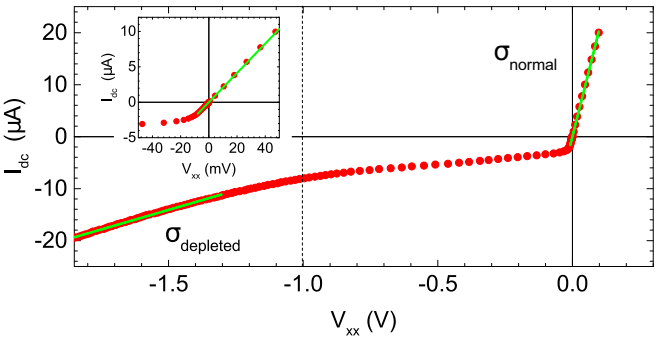

FIG. 4. The dc current I_{dc} as a function of the dc longitudinal voltage drop V_{xx} between the HC 1 and HC 3. The dependence in the normal and depleted regimes ($V_{xx} > -10$ mV and $V_{xx} < -1.2$ V, respectively) are fitted by linear functions in order to get the corresponding electrical conductivities σ_{normal} and σ_{depleted} (fits are depicted by the green lines). Inset: A detail for $V_{xx} > -50$ mV.

The moderately mobile 2DEG that we use has, compared to low-mobility bulk systems, not only a higher σ outside the depleted area, but also a smaller τ_s due to the more effective spin relaxation channels [23,29]. τ_s of the order of tens of picoseconds guarantees, as shown in the 2D spatially resolved responses in Figs. 3(b) and 3(d), the local detection of the spin-polarized current even in a drift electric field of the order of 10^5 Vm^{-1}. This combination of locally sensitive and drift-amplified ISHE response in a system with a moderate overall conductivity allows for the application in spintronic polarimeter devices [30] with a spatial resolution [11].

The local reduction of the carrier concentration, the key functionality of the device, should also affect the spin-transport characteristics. Namely, α_{SH} is expected to decrease with decreasing carrier concentration according to Ref. [16]. To demonstrate this, we need to infer α_{SH} from Eq. (1) in the normal and depleted regime. The corresponding σ in both regimes is inferred from Fig. 4 which displays the evolution of I_{dc} as a function of V_{xx}, i.e., the I/V characteristic of the Hall bar. It clearly shows the high conductive normal regime, unaffected by the p-n junction, with $\sigma_{\text{normal}} = 1.2 \times 10^{-3}$ Ω^{-1}. When the depleted zone edge is expanding through the Hall bar, the conductivity gradually reduces. After the edge exits completely the Hall bar at $V_{xx} < -1.2$ V, the conductivity saturates at $\sigma_{\text{depleted}} = 9.0 \times 10^{-5}$ Ω^{-1}. We use these two values of σ to describe the corresponding regimes.

In order to evaluate α_{SH} from Eq. (1) we have to determine I_s in terms of the photogenerated current I_{pc}. We define $I_s = en_s v$ as the flux of the spin-polarized carriers with drift velocity v and with density $n_s = n^{\uparrow} - n^{\downarrow}$, where $n^{\uparrow}$ and $n^{\downarrow}$ are the total carrier densities of corresponding spins. We can, thus, express

$$I_s = I_{pc} \frac{n_s}{n_p}, \tag{2}$$

where n_p is the concentration of the photogenerated carriers. Upon a continuous illumination with the photocarrier generation rate G, the steady state n_s and n_p follow from the steady state solutions of the rate equations [18,28,31], i.e., $n_s = P_0 G \tau_s$ and $n_p = G\tau$. Here, P_0 is the degree of the spin polarization of the photogenerated electrons and τ is the photocarrier recombination time. In the case of a doped

semiconductor τ_s is not limited by τ since the recombination process involves also the unpolarized electrons from the equilibrium electron population in dark provided by the doping [32–34]. This is why n_s can reach higher values than n_p in doped systems.

As the τ is not experimentally known, we first evaluate the effective spin Hall angle $\tilde{\alpha}_{\mathrm{SH}}$, defined from Eqs. (1) and (2) as

$$\tilde{\alpha}_{\mathrm{SH}} = \alpha_{\mathrm{SH}} \frac{\tau_s}{\tau} = \frac{V_{xy}\sigma}{I_{pc} P_0}. \tag{3}$$

We use V_{xy}, I_{pc}, and $\sigma = \sigma_{\mathrm{depleted}}$ and σ_{normal} corresponding to the fully depleted and normal regimes at $V_{\mathrm{bias}} = -12$ V and $V_{\mathrm{bias}} = +1.3$ V, respectively. We assume $P_0 = 1$ for both the depleted and undepleted regimes, which is the maximum degree of the optically injected spin polarization in 2DEGs at the instant of the photogeneration [18,35,36]. We then get the lower bounds of $\tilde{\alpha}_{\mathrm{SH}}^{\mathrm{depleted}} = (2.7 \pm 0.6) \times 10^{-3}$ for the depleted regime and $\tilde{\alpha}_{\mathrm{SH}}^{\mathrm{normal}} = (7 \pm 2) \times 10^{-2}$ for the undepleted regime. The observed decrease of $\tilde{\alpha}_{\mathrm{SH}}$ by one order of magnitude in the depleted regime compared to the undepleted regime is consistent with the expected behavior from Ref. [16], where the same suppression of α_{SH} is reported over one order of magnitude change in concentration. Considering $\sigma_{\mathrm{normal}}/\sigma_{\mathrm{depleted}} \approx 10$, the carrier concentration in our case also changes by an order of magnitude. In addition, the relative reduction of $\tilde{\alpha}_{\mathrm{SH}}^{\mathrm{depleted}}$ with respect to the normal regime competes with the drift effect on the ISHE signal upon the depletion, suggesting that further optimization of transport parameters could bring even a more efficient amplification of the electrical ISHE signal in the depleted regime.

Values of α_{SH} reported in bulk and similar low dimensional systems [10,12,16,37] do not usually exceed 10^{-2}. This is consistent with our values of $\tilde{\alpha}_{\mathrm{SH}}$ if $\tau < \tau_s \sim 10$ ps, which would be an indication of highly effective photocarrier recombination. These values of τ can be found in GaAs at low temperatures, especially if trapping processes are significant [38–42].

V. CONCLUSION

In conclusion, we have demonstrated that the large, bias-controlled expansion of the depleted zone in a lateral *p-n* junction can be used to amplify the electrically detected ISHE signals by more than one order of magnitude with respect to the unbiased regime. In this device, the source and drain contacts are used both to apply the drift bias and to deplete the carrier density in the Hall bar by the expanding depletion zone, whose width is spatially controlled with submicrometer resolution. Due to the low-dimensional nature of the sample, the reduced spin life-time and the corresponding spin drift-length allow us to perform local detection of spin currents even in a high electric field of the order of 10^5 Vm^{-1}. The gatinglike effect of the device affects the spin Hall angle consistently with the previous reports and gives the perspective of a further optimization of the spin Hall device. The combination of the ISHE signal amplification by the drift and depletion functionalities, together with the local character of the spin detection guaranteed in a wide range of drift conditions, is promising for concepts of ISHE-based spintronic devices, such as spintronic polarimeters.

ACKNOWLEDGMENTS

We acknowledge support from the European Research Council (ERC) Advanced Grant No. 268066, from the European Metrology Research Programme within the Joint Research Project EXL04 (SpinCal), from the Ministry of Education of the Czech Republic Grant No. LM2015087, from the Czech Science Foundation Grant No. 14-37427G, and from the Charles University Grants No. 1360313 and No. SVV-2015-260216.

[1] Y. K. Kato, R. C. Myers, A. C. Gossard, and D. D. Awschalom, Science **306**, 1910 (2004).
[2] J. Wunderlich, B. Kaestner, J. Sinova, and T. Jungwirth, arXiv:cond-mat/0410295 (2004).
[3] J. Wunderlich, B. Kaestner, J. Sinova, and T. Jungwirth, Phys. Rev. Lett. **94**, 047204 (2005).
[4] S. O. Valenzuela and M. Tinkham, Nature (London) **442**, 176 (2006).
[5] E. Saitoh, M. Ueda, H. Miyajima, and G. Tatara, Appl. Phys. Lett. **88**, 182509 (2006).
[6] H. Zhao, E. J. Loren, H. M. van Driel, and A. L. Smirl, Phys. Rev. Lett. **96**, 246601 (2006).
[7] T. Jungwirth, J. Wunderlich, and K. Olejník, Nat. Mater. **11**, 382 (2012).
[8] I. M. Miron, K. Garello, G. Gaudin, P.-J. Zermatten, M. V. Costache, S. Auffret, S. Bandiera, B. Rodmacq, A. Schuhl, and P. Gambardella, Nature (London) **476**, 189 (2011).
[9] L. Liu, C.-F. Pai, Y. Li, H. W. Tseng, D. C. Ralph, and R. A. Buhrman, Science **336**, 555 (2012).
[10] J. Wunderlich, A. C. Irvine, J. Sinova, B. G. Park, L. P. Zârbo, X. L. Xu, B. Kaestner, V. Novák, and T. Jungwirth, Nat. Phys. **5**, 675 (2009).
[11] L. Nádvorník, J. A. Haigh, K. Olejník, A. C. Irvine, V. Novák, T. Jungwirth, and J. Wunderlich, Phys. Rev. B **91**, 125205 (2015).
[12] K. Olejník, J. Wunderlich, A. C. Irvine, R. P. Campion, V. P. Amin, J. Sinova, and T. Jungwirth, Phys. Rev. Lett. **109**, 076601 (2012).
[13] J. Wunderlich, B. G. Park, A. C. Irvine, L. P. Zârbo, E. Rozkotová, P. Nemec, V. Novák, J. Sinova, and T. Jungwirth, Science **330**, 1801 (2010).
[14] V. K. Gurugubelli and S. Karmalkar, J. Appl. Phys. **118**, 034503 (2015).
[15] Z. L. Wang and W. Wu, Natl. Sci. Rev. **1**, 62 (2014).
[16] S. Matsuzaka, Y. Ohno, and H. Ohno, Phys. Rev. B **80**, 241305 (2009).
[17] The slow time-etching using the 0.2% solution of H_3PO_4 provided the precision of a few nanometers.
[18] V. M. Agranovich, F. Meier, B. P. Zakharchenya, and A. A. Maradudin, in *Optical Orientation*, edited by F. Meier and B. P. Zakharchenya, Modern Problems in Condensed Matter Sciences Vol. 8 (Elsevier Science, Amsterdam, 1984).
[19] S. Nemoto, Appl. Opt. **28**, 1643 (1989).
[20] D. Reuter, C. Werner, A. D. Wieck, and S. Petrosyan, Appl. Phys. Lett. **86**, 162110 (2005).

[21] Note that in the specific measurements in Fig. 2(b) the signal at HC 2 is fully saturated while at HC 1 and HC 3 V_{xy} shows a residual weak bias dependence in the saturated region. The detailed behavior in the saturated region depends on the precise alignment of the laser spot on top of each HC and, therefore, can vary between the measurements.
[22] M. I. Miah, J. Phys. D **40**, 1659 (2007).
[23] M. Wu, J. Jiang, and M. Weng, Phys. Rep. **493**, 61 (2010).
[24] E. Hecht and A. Zajac, *Optics*, 2nd ed. (Addison-Wesley, Reading, MA, 1987).
[25] We note that we had to significantly increase the spot size by using less collimated light in order to suppress the effect of the spatial motion of the (nominally nonmagnetic) objective by $\sim$1 μm due to its interaction with the magnetic field. Using the larger spot we eliminated this experimental artifact.
[26] K. Ando and E. Saitoh, Nat. Commun. **3**, 629 (2012).
[27] F. Bottegoni, A. Ferrari, G. Isella, M. Finazzi, and F. Ciccacci, Phys. Rev. B **88**, 121201 (2013).
[28] N. Okamoto, H. Kurebayashi, T. Trypiniotis, I. Farrer, D. A. Ritchie, E. Saitoh, J. Sinova, J. Mašek, T. Jungwirth, and C. H. W. Barnes, Nat. Mater. **13**, 932 (2014).
[29] J. Zhou, J. L. Cheng, and M. W. Wu, Phys. Rev. B **75**, 045305 (2007).
[30] The ISHE-based polarimeter is a new solid-state polarimeter concept that can provide, compared to the classical polarimeter setups based on a set of crossed polarizers, a faster operation rate, microsized dimensions and possible integration into chiplike devices. More details can be found in Ref. [11].
[31] M. I. Dyakonov, *Spin Physics in Semiconductors*, 1st ed. (Springer, Berlin, 2008).
[32] R. I. Dzhioev, K. V. Kavokin, V. L. Korenev, M. V. Lazarev, B. Y. Meltser, M. N. Stepanova, B. P. Zakharchenya, D. Gammon, and D. S. Katzer, Phys. Rev. B **66**, 245204 (2002).
[33] J. M. Kikkawa and D. D. Awschalom, Phys. Rev. Lett. **80**, 4313 (1998).
[34] G. Salis, A. Fuhrer, R. R. Schlittler, L. Gross, and S. F. Alvarado, Phys. Rev. B **81**, 205323 (2010).
[35] B. Dareys, X. Marie, T. Amand, J. Barrau, Y. Shekun, I. Razdobreev, and R. Planel, Superlattices Microstruct. **13**, 353 (1993).
[36] S. Pfalz, R. Winkler, T. Nowitzki, D. Reuter, A. D. Wieck, D. Hägele, and M. Oestreich, Phys. Rev. B **71**, 165305 (2005).
[37] E. S. Garlid, Q. O. Hu, M. K. Chan, C. J. Palmstrøm, and P. A. Crowell, Phys. Rev. Lett. **105**, 156602 (2010).
[38] K. Fukumoto, Y. Yamada, S.-y. Koshihara, and K. Onda, Appl. Phys. Express **8**, 101201 (2015).
[39] S. Gupta, M. Y. Frankel, J. A. Valdmanis, J. F. Whitaker, G. A. Mourou, F. W. Smith, and A. R. Calawa, Appl. Phys. Lett. **59**, 3276 (1991).
[40] K. A. McIntosh, K. B. Nichols, S. Verghese, and E. R. Brown, Appl. Phys. Lett. **70**, 354 (1997).
[41] S. S. Prabhu, S. E. Ralph, M. R. Melloch, and E. S. Harmon, Appl. Phys. Lett. **70**, 2419 (1997).
[42] P. W. E. Smith, S. D. Benjamin, and H. S. Loka, Appl. Phys. Lett. **71**, 1156 (1997).